Dynamics of laser buildup from quantum noise

F. T. Arecchi,* W. Gadomski,[†] R. Meucci, and J. A. Roversi[‡]

Istituto Nazionale di Ottica, 50125 Firenze, Italy

(Received 7 July 1988)

We measure the statistical distribution of buildup times for the field of a single-mode CO_2 laser when cavity losses have rapidly changed from a large to a small value. The ratio between the average buildup time and its statistical spread is shown to be a sensitive test of the quantum fluctuations in the off state. This method operates as a "statistical microscope," permitting the accurate determination of a small mean photon number in the infrared region by optical amplification, and a discrimination of the initial mean photon number from noise contributions along the amplification process. Following the buildup, the laser pulse decays on two time scales. The faster one, due to the radiation coupling, can be fitted by a Toda oscillator model; the slower one, due to the collisional dynamics of the excited population, provides a quantitative evaluation of two distinct population decay rates, one within the rotational manifold and the other one out of the vibrational band.

I. INTRODUCTION

The first observation of a statistical spread in the leading edge of a Q-switched laser pulse was associated with the appearance of a large peak in the variance of the transient photon number distribution.[1] This fact was explained in terms of an approximately deterministic decay out of a macroscopic unstable state, to be averaged over the statistical distribution of the initial states.[1,2] Such behavior was later shown to be peculiar of quenching phenomena in macroscopic systems, such as spinodal decomposition in thermodynamic systems.[3]

As stressed by Haake,[4] this phenomenon is the transient counterpart of the stationary fluctuations at the critical point of a thermodynamic phase transition (or more generally at the bifurcation points in a nonlinear dynamics which display the same formal features of a second-order phase transition). Precisely, if we call N the number of degrees of freedom of a macroscopic system decaying out of an unstable state, the initial fluctuations are of the order of $1/N$ $[O(1/N)]$, however, in the linear part of the decay they are amplified by $O(N)$, hence the relative fluctuations are of $O(1)$.

The assumption of deterministic evolution out of a spread initial state neglected the role of fluctuations along the build up with respect to the initial ones. The relation between the two types of noise were explored in a series of papers by Suzuki, summarized at the XVII Solvay Conference of Physics.[5] In that conference, a remark by P. Martin to Arecchi[6] reopened the question of the nature of these large fluctuations.

Upon Martin's remark a quest for a discrimination between fluctuations on the initial condition and those along the path led to a new observation method, based on the statistics of passage times at a given threshold.[7,8] From this method it resulted clearly that, when a laser is suddenly switched far above threshold, the fluctuations are mainly due to the initial spread, as already guessed in Refs. 1 and 2. This method of passage time provided an important difference between gas and dye lasers,[9] since in

the latter case it permitted detection of the role of pump fluctuations as "noise along the path."[9,10]

Both the He-Ne and the dye laser have in common a population decay rate large with respect to the photon decay rate (so called class-A lasers[11]). Hence the population adiabatically follows the intensity changes, with a consequent reduction of inversion as the cavity losses are lowered. This adiabatic following forbids any overshoot in the laser intensity. Indeed, Q switching in class-A lasers is characterized by an intensity monotonically increasing up to an asymptotic value. In contrast, when the population decay is slower than the photon decay (class-B lasers[11]) the initially large population storage provides a large intensity pulse by stimulated emission, and only later the population feels the slower depletion channels (either spontaneous emission in ruby and semiconductors, or collisional deexcitations in CO_2). This explains why, after a sudden loss reduction, class-B lasers release giant intensity pulses well above the asymptotic value, whereas class-A lasers do not.

We generate transient dynamics in a single-mode CO_2 laser by switching an intracavity modulator from absorption to transparency in a time shorter than the build up time of the giant pulse. We summarize below the main results, to be discussed in this paper.

(i) With respect to the start pulse (zero time), the modulator switching lasts for a time (~ 1.0 μs) much shorter than the average buildup time (around 3 μs). The average spread $\overline{\delta t}$ of the leading front (jitter) is around 0.2 μs.

(ii) If we consider the time t_1 necessary to reach a photon number n_1 still below the saturation value n_s ($n_1 = 0.5 n_s$), the laser dynamics up to t_1 can be taken as linear. In this linear regime, a simplified version of passage time statistics[12] leads to a very powerful relation which permits evaluation of the effective seeding photon number at the onset of the dynamics in terms of the threshold photon number n_1 and of the ratio of the average $\overline{t_1}$ the spread $\overline{\delta t}$. Our method is self-calibrating, in the sense that the second moment of the observed statis-

tics provides the amplification gain without any previous calibration, and the higher-order cumulants provide the error bars of the experimental points.

(iii) We can detect a few initial photons in a laser cavity by linear optical amplification. The reported amplification factors are of the order of 10^8, but in principle they could be larger. The linearity of the amplification process is preserved up to the saturation photon number, which is over 11 decades in our case.

(iv) While in a class-A laser the photon population reaches a maximum and remains clamped to that value, in a class-B laser the photon-population interaction leads to fast dynamics yielding a short pulse. During this pulse, the population inversion is practically decoupled from its thermal reservoir, and its evolution depends only on the coupling with the radiation field. With this assumption, the pulse shape can be fitted by a Toda oscillator model.[13]

(v) The long-time characteristics of the emitted radiation are affected by the interaction of the population inversion with its thermal reservoir. Among the class-B lasers with long population decay times, we must introduce a further distinction between B_1, where radiators are modeled as two-level atoms, and B_2, where the radiative transition has a fast coupling with another manifold, and this manifold on its turn has a slower coupling with the thermal reservoir (four-level atoms). This latter model was introduced by Dupré et al.[14] and extensively used by Arimondo and co-workers in connection with saturable absorbers.[15,16] Our experiments show that a class B_1 model is inadequate for a CO_2 laser, which in fact is a class-B_2 laser. The corresponding model parameters are accurately fitted by the long-time tail of our laser. Thus our data provide a direct quantitative measurement of the CO_2 molecular parameters. A preliminary report of cases (i) to (iii) was given in Ref. 17. In Sec. II we discuss the experiment and present the data; Sec. III is devoted to theory and data interpretation of the leading edge [cases (i) to (iii)]; Sec. IV deals with the giant pulse formation [case (iv)]; finally Sec. V discusses the long-time behavior and the difference between class-B_2 and -B_1 lasers [case (v)].

II. EXPERIMENTAL RESULTS

The experimental set up Fig. 1 consists of a single-mode CO_2 laser with an intracavity electro-optic modulator (EOM). Details on the dynamics of the CO_2 laser and on our laboratory system can be found in a review paper.[18] The cavity consists of a grating blazed for 10.6 μm (P20 line) and a fully reflecting spherical mirror. Light output is obtained via an intracavity beam splitter with 5% reflectance.

The gas cell is terminated by Brewster windows. When voltage is applied to the EOM, this rotates the polarization plane thus increasing the intracavity losses. The gas mixture (CO_2:N_2:He$=1$:1:7) is at a total pressure of 20 torr. Since the collisional broadening is around 7 MHz/torr, the collisional width is about larger by 100 MHz than the Doppler line (50 MHz). Thus the gain line is homogeneously broadened.
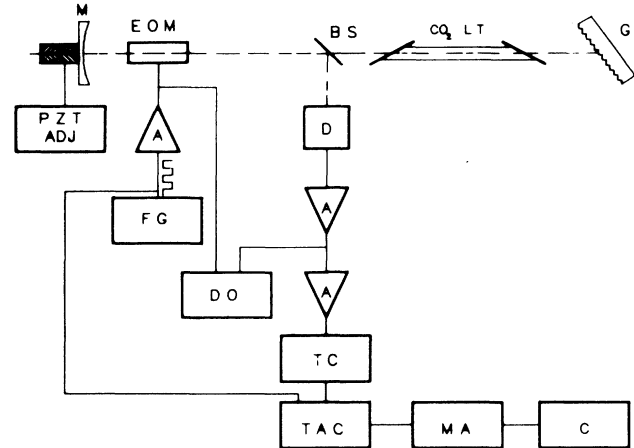

FIG. 1. Experimental setup with a CO_2 laser. M represents the total reflecting mirror mounted on a piezo translator, G represents the grating (100 lines/mm), BS represents the ZnSe beam splitter, EOM represents the electro-optic modulator, D represents the $Hg_x Cd_{1-x}$Te detector, A represents the amplifier, FG represents the function generator (square wave), DO represents the digital oscilloscope, TC represents the threshold circuit, TAC represents the time to amplitude converter, MA represents the multichannel analyzer, and C represents the computer.

As we switch the EOM voltage from about 800 to 130 V, the cavity loss rate k decreases from k_0 to k_1 with a time constant of 0.79 μs as shown in Fig. 2. A laser pulse builds from a low photon number n_0 (laser below threshold for loss k_0) up to a peak value at $\bar{t} \sim 3$ μs. The pulse develops over a time much shorter than the fastest decay rate of the population,[14] thus the population change during the pulse is mainly due to the radiative interaction. We notice from Fig. 2 that the time jitter already present in the first part of the leading edge is preserved along the whole pulse. This means that the various trajectories are shifted versions of the same deterministic curve, and the noise plays a role only in spreading the initial condition.[7]
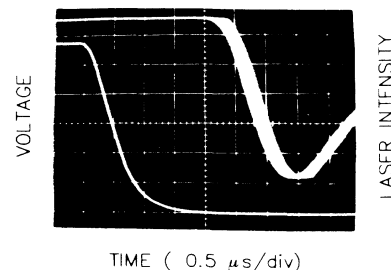

TIME (0.5 μs/div)

FIG. 2. Oscilloscope plots of the EOM voltage driven from $V_0 = 710$ V to $V_1 = 130$ V and of a set of transient intensity traces starting from the off state. The time jitter is uniform along the evolution. To avoid the role of nonlinearities, the threshold n_1 for the time distribution $p(t_1)$ (see Fig. 2) is adjusted below the saturation photon number, that is, rather close to the off state (at just 10% of the peak intensity). The discharge current is 3.377 mA.

We will see indeed that all fluctuations can be attributed to an equivalent noise.

In order to remain in the linear regime we consider the evolution up to t_1 when the photon number n_1 is smaller than the saturation value[18] n_s, precisely

$$n_1 = 0.5 n_s .$$

Up to t_1, we can take the population inversion as fixed at the prepulse value z_0.

As can be seen qualitatively in Fig. 2, superposition of many successive pulses shows a spread in the buildup time, with an average spread $\overline{\delta t}$ much smaller than $\overline{t_1}$. Indeed, by setting a threshold circuit on the photodetector output at $n = n_1$ and then using a time-to-amplitude converter, we can measure the statistical distribution of times of arrival to the photon number n_1. An example is shown in Fig. 3. From this we can evaluate first and second moment and measure accurately $\overline{t_1} = \langle t_1 \rangle$ and $\overline{\delta t} = \langle t^2 \rangle^{1/2}$. A set of experimental data, including skewness and kurtosis of the statistical time distributions, is reported in Table I.

As discussed in Sec. III, the aim of these observations of transient statistics is the discrimination between the initial photon number $\langle n_0 \rangle$ before the Q switch and the "noise along the path" n_p, that is, the equivalent photon number corresponding to spontaneous emission fluctuations during the amplifying process. To evaluate these parameters we need, besides the measurement of the cumulants of $p(t_1)$, an accurate calibration of loss rate $k(t)$, in order to assign initial (k_0) and final (k_1) cavity loss rates, and power output P, in order to assign the threshold photon number n_1.

The EOM relation is

$$k(t) = \overline{k} \left[1 + \alpha \sin^2 \left| \frac{V(t) - \overline{V}}{V_{\lambda/2}} \right| \right] , \qquad (1)$$

where $V_{\lambda/2} = 4240$ V is the $\lambda/2$ voltage (maximum rotation of the polarization plane across the EOM crystal). α and $\overline{V}$ [dephasing at $V(t) = 0$] are fitted with a 30-point calibration of the EOM transmission giving values $\alpha = 4.62$ and $\overline{V} = 206$ V. Finally, $\overline{k} = 2 \times 10^7$ s^{-1} is the

TABLE I. First four cumulants of $p(t_1)$ (see Fig. 2). Acquisition time 300 s. Since we collect 150 data per second the total number of counts is 4.5×10^4. K_1, K_2, K_3 (expt.), and K_4 (expt.) are measured values; K_3 (theor.) and K_4 (theor.) are obtained from Eq. (1) where W is expressed only in terms of $\overline{t_1} = K_1$ and $\overline{\delta t} = K_2^{1/2}$, without any other knowledge of model-dependent parameters.

K_1 (μs)	K_2 ($\times 10\ \mu$s^2)	K_3 ($\times 10^3\ \mu$s^3) expt.	theor.	K_4 ($\times 10^4\ \mu$s^4) expt.	theor.
2.44	1.21	1.29	1.52	0.26	0.35

most accurate value resulting from loss calibration. An independent criterion which gives the same $\overline{k}$ value is discussed in Sec. III.

The proportionality between laser power output and discharge current is shown in the experimental plot of Fig. 4. This permits a precise localization of the threshold point.

Figure 5 gives the pulse evolution when the laser starts from an above-threshold state. In such a case the evolution is practically deterministic (no jitter) as shown by the superposition of 10^4 successive transients. Figure 6 is the evolution of a single transient over long times. Besides the giant pulse, already visible in Fig. 2 and 5, we report here the trailing edge ending in a steady state.

From the point of view of power assignment, the vertical axis of Fig. 4 is calibrated in values of the steady-state power. Indeed, the pulse area is so small that it practically gives no contribution to the power measurement. The peak power is then inferred from the ratios of peak to plateau height. The threshold value of $n_1 = 1.70 \times 10^{11}$ is accurate within 1%.

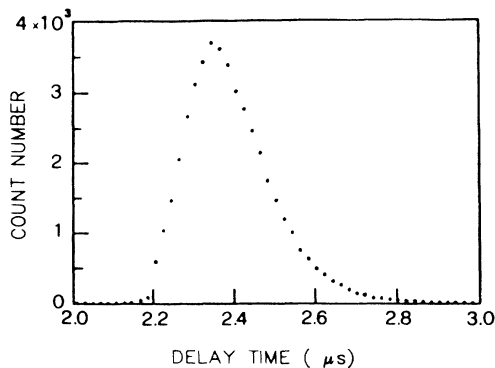A key point of our approach is that, by use of our sta-

FIG. 3. Statistical distribution $p(t_1)$ of the passage times through the threshold photon number $n_1 = 0.5 n_s$. This distribution corresponds to the same parameter values of Fig. 2.
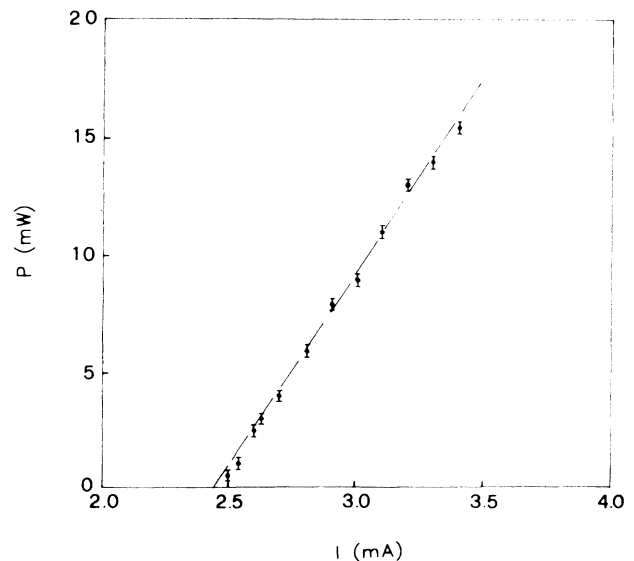

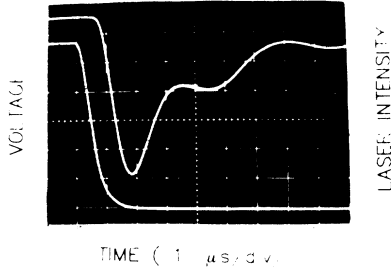FIG. 4. Laser power vs discharge current in the operating regime.

FIG. 5. Time development of laser pulses from low to high coherent emission (above-threshold switch). The exposure corresponds to 10^4 successive transients and it shows no jitter. The discharge current is 3.913 mA.

tistical method we will obtain (Sec. III) rather good determinations of photon numbers around 10^3 starting from a *direct* measurement of the much larger n_1, which is easily accessible to standard photodetectors in the 10-μm region.

III. TRANSIENT STATISTICS

A. Theory

Since photon counting measurements deal with normal ordered averages, by exploiting the quantum-classical correspondence,[19] we deal directly with a classical field amplitude α and its corresponding probability density $P(\alpha)$.

Having limited the evolution to the linear regime (no population depletion) the field dynamics is ruled by a linear Langevin equation

$$\dot{\alpha} = \tfrac{1}{2}a\alpha + \xi(t) .\tag{2}$$

Here the rate coefficient $\tfrac{1}{2}a$ is the net field gain, and the factor $\tfrac{1}{2}$ accounts for the difference between field and photon rate, that is,

$$a(t) = Gz_0 - k(t) ,\tag{3}$$

where G is the stimulated emission coefficient for the P20 transition at 10.6 μm, z_0 is the population inversion imposed by the pump (and kept unperturbed during the
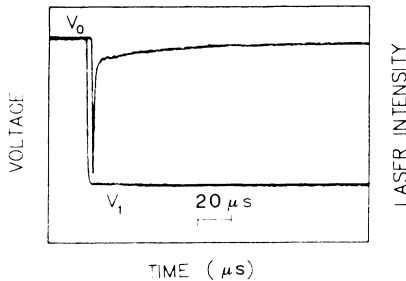

FIG. 6. Time development of a single transient over long times. Time scale 20 μs/div.

linear amplification regime), and $k(t)$ is the cavity loss rate, decreasing from k_0 to k_1. G is given by[18]

$$G = \frac{\omega\mu^2}{\gamma_\perp \hbar\varepsilon_0 V} ,\tag{4}$$

where $\mu^2/\hbar\varepsilon_0$ (μ^2 being the dipole matrix element) is evaluated from the spontaneous emission rate γ_{sp} for the transition[20]

$$\gamma_{sp} = \frac{8\pi}{3}\frac{\mu^3}{\hbar\varepsilon_0\lambda^3} = 0.3 \text{ s}^{-1} .$$

Taking into account that the cavity volume, for a cavity length $L = 200$ cm and for a near confocal configuration, is given by $V = L^2\lambda = 40$ cm^3, and that, since we have a total gas pressure of 20 torr and a collisional broadening[20] of 7 MHz/torr,

$$\gamma_\perp = 140\pi = 4.4 \times 10^8 \text{ s}^{-1} ,$$

it follows $G = 3.8 \times 10^{-7}$ s^{-1}.

Let us now consider a sudden switch at $t = 0$ from $k_0 > Gz_0$ to $k_1 < Gz_0$. The noise source $\xi(t)$ is a zero-average, δ-correlated Gaussian process

$$\langle \xi(t)\xi(t')\rangle = D\delta(t - t') ,\tag{5}$$

where the diffusion constant D is due to the spontaneous photon generation into the cavity mode. In the far-infrared region we should also account for a thermal (blackbody) contribution. However, for $\lambda = 10$ μm this becomes important only for an initial photon number $n_0 < \frac{1}{20}$ and we show that we never reach such a limit in these experiments.

For $t \le 0$ the laser is at equilibrium below threshold with a photon number

$$\langle n_0\rangle = \langle |\alpha_0|^2\rangle = \frac{D}{|a_0|} + n_{th} ,\tag{6}$$

where $a_0 = k_0 - Gz_0$, and n_{th} is the blackbody contribution given by Planck equation,

$$n_{th} = (e^{\hbar\omega/kT} - 1)^{-1} .\tag{7}$$

Here, T coincides practically with the discharge temperature, since the cavity is almost completely filled by the discharge tube.

Calling N_2 the total population of the upper laser level and η an angular coupling efficiency, we have

$$D = \gamma_{sp}N_2\eta ,\tag{8}$$

where

$$\eta = \frac{\Omega}{4\pi} = \frac{\gamma}{4\pi L} \simeq 10^{-6} .\tag{9}$$

The time-dependent probability density is given by

$$P(\alpha) = \left\langle \frac{1}{\pi\dfrac{D}{a}(e^{at} - 1)}\exp\left[-\frac{|\alpha - \alpha_0 e^{at/2}|^2}{\dfrac{D}{a}(e^{at} - 1)}\right]\right\rangle_{\alpha_0} ,\tag{10}$$

where the average has to be performed over the initial Gaussian field distribution

$$P(\alpha_0) = \frac{1}{\pi \langle n_0 \rangle} \exp \left[-\frac{|\alpha_0|^2}{\langle n_0 \rangle} \right] \qquad (11)$$

and $a = Gz_0 - k_1$ is the field rate for $t > 0$.

In the linear case, we can account for both the initial uncertainty given by (11), as well as the noise amplification along the path given by Eq. (10), in a simple way.[21] Indeed, for $e^{at} \gg 1$, we can approximate Eq. (10) as

$$P(\alpha) = e^{-at} \left\langle \frac{1}{\pi \frac{D}{a}} \exp \left[-\frac{|\alpha - \alpha_0 e^{at/2}|^2}{\frac{D}{a} e^{at}} \right] \right\rangle_{\alpha_0} \qquad (12)$$

If now we introduce the auxiliary variable α' such that $\alpha' = \alpha e^{-at}$, then

$$d^2\alpha' = e^{-at} d^2\alpha , \qquad (13)$$

and Eq. (10) can be formally written as

$$P(\alpha) = \int \delta^{(2)}(\alpha - \alpha' e^{at/2})$$

$$\times \left\langle \frac{1}{\pi \frac{D}{a}} \exp \left[-\frac{|\alpha' - \alpha_0|^2}{\frac{D}{a}} \right] \right\rangle_{\alpha_0} d^2\alpha' . \qquad (14)$$

This is the deterministic evolution, noise free, of the initial distribution $\tilde{P}(\alpha')$ given by the brackets, which on its turn is a convolution of two Gaussians

$$\tilde{P}(\alpha') = \int \frac{1}{\pi \frac{D}{a}} \exp \left[-\frac{|\alpha' - \alpha_0|^2}{\frac{D}{a}} \right] \frac{1}{\pi \langle n_0 \rangle}$$

$$\times \exp \left[-\frac{|\alpha_0|^2}{\langle n_0 \rangle} \right] d^2\alpha_0$$

$$= \frac{1}{\pi \left[\frac{D}{a} + \langle n_0 \rangle \right]} \exp \left[-\frac{|\alpha'|^2}{\frac{D}{a} + \langle n_0 \rangle} \right] . \qquad (15)$$

Thus the equivalent initial distribution which then evolves deterministically is a Gaussian one, with a total equivalent photon number given by

$$N_0 = \frac{D}{a} + \langle n_0 \rangle = n_p + \langle n_0 \rangle \qquad (16)$$

As discussed in correspondence of Eqs. (5) and (6), D contains both the spontaneous and the blackbody contributions. Separating as in Eq. (6) we can rewrite N_0 as

$$N_0 = \frac{D}{a} + \frac{D}{|a_0|} + 2n_{\text{th}} , \qquad (17)$$

where D is given by Eq. (8). No further consideration will be payed to n_{th} in this paper, and we skip it from Eq. (6) and (17), in view of the negligible contribution of the n_{th} to $\langle n_0 \rangle$. The situation is drastically different in the far-infrared region, and we plan to extend these investigations in that spectral region.

Now we give up with the ideal case of step like switch, and consider the real situation of a loss rate $k(t)$ decreas-

ing from k_0 to k_1 with a time constant τ, as shown in Fig. 2. The evolution rate of the Langevin equation becomes then

$$a(t) = a_0 + (k_0 - k_1)(1 - e^{-t/\tau}) . \qquad (18)$$

The deterministic part of Eq. (2) yields a simple equation for the photon number $n = |\alpha|^2$,

$$\dot{n} = a(t)n , \qquad (19)$$

whose integration yields the time t_1 at which the photon number reaches the value n_1,

$$\ln \frac{n_1}{n_0} = \int_0^{t_1} a(t)dt = at_1 - (k_0 - k_1)\tau(1 - e^{-t_1/\tau}) , \qquad (20)$$

where $a = Gz_0 - k_1$ is the final value of the net gain.

For simplicity, we introduce the auxiliary variable

$$t_s = \frac{\Delta k}{a} \tau(1 - e^{-t_1/\tau}) , \qquad (21)$$

which depends weakly on t_1. Since in all experimental situations considered $\bar{t}_1 \gg \tau$ ($\bar{t}_1$ is the average of t_1), the small correction $e^{-t_1/\tau}$ will be replaced by $e^{-\bar{t}_1/\tau}$. This way, t_s no longer depends on t_1, and we can invert the relation $n_0 = n_0(t_1)$ as follows:

$$t_1(n_0) = t_s + \frac{1}{a} \ln \frac{n_1}{n_0} . \qquad (22)$$

The passage time t_1, as a function of the equivalent initial photon number n_0 [equivalent, because it accounts also for noise along the path, ruled out in the deterministic solution Eq. (20)], has a statistics given by

$$p(t_1) = \int \delta(t_1 - t_1(n_0))p(n_0)dn_0 , \qquad (23)$$

where

$$p(n_0) = \frac{1}{N_0} e^{-n_0/N_0} , \qquad (24)$$

the average N_0 being given by Eq. (16). It is now convenient to introduce a moment-generating function[12]

$$W(\lambda) = \int_0^\infty e^{-\lambda t} p(t_1)dt_1 . \qquad (25)$$

From Eqs. (22)–(24) it follows that

$$W(\lambda) = e^{-\lambda t_s} \int_0^\infty \left[\frac{n_0}{n_1} \right]^{\lambda/a} e^{-n_0/N_0} \frac{dn_0}{N_0}$$

$$= e^{-\lambda t_s} \left[\frac{n_1}{N_0} \right]^{-\lambda/a} \Gamma(\lambda/a + 1) . \qquad (26)$$

From this we have

$$\bar{t}_1 = \langle t_1 \rangle = -\frac{d}{d\lambda} \ln W \bigg|_{\lambda=0} = \frac{1}{a} \left[\ln \frac{n_1}{N_0} - \Psi(1) \right] + t_s , \qquad (27)$$

$$\overline{(\delta t)^2} = \langle \Delta t^2 \rangle = \frac{d^2}{d\lambda^2} \ln W \bigg|_{\lambda=0} = \frac{1}{a^2} \Psi'(1) , \qquad (28)$$

and in general the K_n cumulant is given by

$$K_n = (-1)^n \frac{1}{a^n} \psi^{n-1}(1) ,$$ (29)

where $\psi^{n-1}(1)$ is the polygamma function.[22]

B. Interpretation of data

Notice that Eq. (27), written as

$$N_0 = n_1 \exp\{-[a(\overline{t_1}-t_s)+\Psi(1)]\} ,$$ (30)

is the formal integral of Eq. (19) where, apart from the constant corrections t_s and $\Psi(1)$, the average equivalent initial condition N_0 is expressed in terms of the measured threshold value n_1 and the average time t_1. Furthermore, Eq. (28) provides a model-independent way of evaluating the gain $a = [\Psi'(1)]^{1/2}/\delta t$. Once this evaluation is introduced into Eq. (29) for $n > 2$, the corresponding theoretical cumulants can be compared with the measured values. This is shown in Table I with reference to the distribution of Fig. 3.

In Table II and Figs. 7 and 8 we give data for three experimental situations, corresponding to the same initial photon number $\langle n_0 \rangle = D/|a_0|$, that is (see inset in Fig. 7), same discharge current and initial EOM voltage $V_0 = 778$ V. The three situations are characterized by different final EOM voltages V_1, as listed in Table II, first row.

By measuring the first two cumulants K_1 and K_2 of the time statistics, we retrieve the values of the $\overline{t}$ and δt, respectively. Thus by use of the "statistical microscope," Eq. (30), we evaluate N_0 (fifth row of Table II). By knowledge of a_0 and hence of $\langle n_0 \rangle$, we isolate the "noise along the path" $n_p = N_0 - \langle n_0 \rangle$, as given in part (b) of Fig. 8. The associated error bars are discussed below [see Eqs. (31)–(35)].

The diffusion coefficient D (last row of Table II) is eventually calculated from Eq. (17). In fact Eq. (17) was deduced in the instant sweep limit, that is, for $t_s \to 0$, however, a finite t_s contributes a rigid translation in Eq. (30), but it does not affect D, as was shown in a recent theory of a finite sweep[23] and as can be easily proved by a straightforward numerical integration of the transient equations, without any approximation. More precisely, Eq. (3.12) of Ref. 23 yields the equivalent initial photon
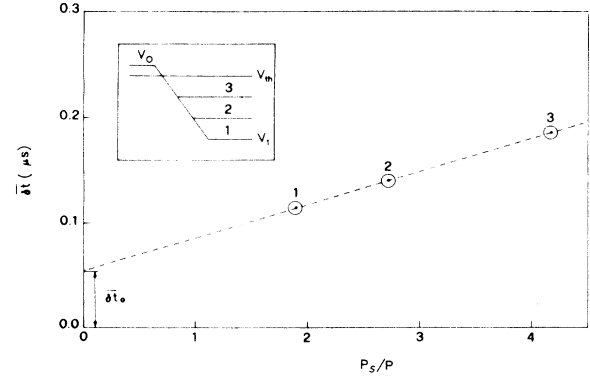

FIG. 7. Plot of the average time spread $\overline{\delta t}$ vs the reciprocal of the output power P. P is evaluated for long times, after the transient has died out, the normalization P_s is the saturation power. The error bars are smaller than the dots (the circles around the dots are just indicators). The intercept $\overline{\delta t_0}$ is the asymptotic uncertainty for large powers. The inset shows the relative EOM voltage settings in the three experiments (V_0 and V_1 represent the initial and final voltages, respectively, V_{th} represents the threshold voltage).

number for a finite sweep time, under two assumptions: (i) the sweep is linear in time $a(t) = a_0 + \lambda t$ and (ii) the small-noise limit, that is, $D \ll \sqrt{\lambda}$ (we call here λ the linear slope which in our case would be $\lambda = \Delta k / t_s$). In fact neither (i) nor (ii) hold in our experiment and that result is not fully applicable. However, to check the sensitivity of N_0 to the duration t_s of the sweep time, we have inserted our experimental data (from column 1 of Table II) into Eq. (3.12) of Ref. 23. We then calculate
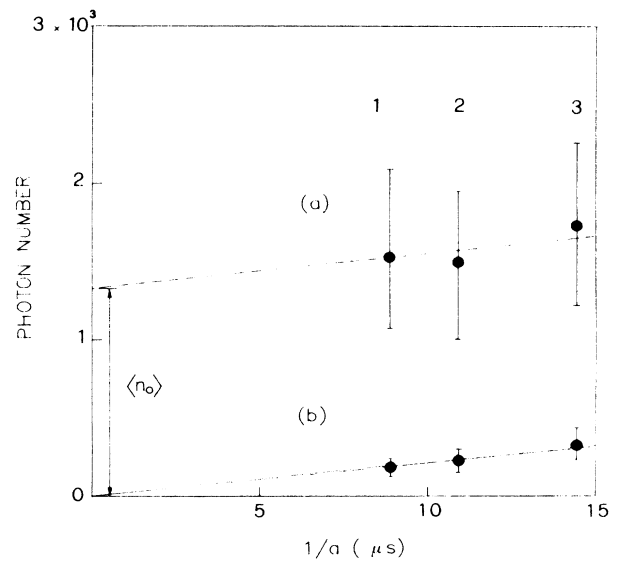
TABLE II. Numerical values for the three experiments of Figs. 7 and 8. Values of V_0, V_{th}, $|a_0|$, and τ are kept constant for the three experiments and equal to 778 V, 746 V, 1.6 (10^6 s^{-1}), and 0.6 μs, respectively.

	Experiment		
	1	2	3
V_1 (V)	420	520	595
$\overline{t_1}$ (μs)	2.39	2.79	3.48
$\overline{\delta t}$ (μs)	0.115	0.140	0.185
a (10^{-6} s^{-1})	11.13	9.14	6.92
N_0	1533	1504	1735
n_p	194	225	327
D (10^{-9} s^{-1})	2.15	2.05	2.26

FIG. 8. Total photon number N_0 (a) and equivalent photon number n_p corresponding to noise along the path (b) vs the reciprocal of the gain rate a. The vertical intercept of N_0 for $1/a = 0$ is the initial photon number $\langle n_0 \rangle$.

$D \simeq 2 \times 10^9$ s^{-1} against our tabular value $D = 2.15 \times 10^9$ s^{-1}. Thus D seems not affected by a finite rise time. To prove this experimentally, we have increased the time constant of the EOM pulse from $\tau = 0.6$ μs up to $\tau = 2$ μ s. Whenever we perform measurements at $t_1 \geq 2\tau$ we do not measure any substantial change in $\overline{\delta t}$, that is, the finite sweep, provided it is shorter than the lethargy time, affects only the first cumulant, as accounted for in Eq. (30).

In Fig. 7, the average spreads $\overline{\delta t}$ are reported versus the reciprocal of the output power P. Since Eq. (28) yielded the simple relation $\overline{\delta t} = 1.28/a$ and in the linear regime P grows as a, $\overline{\delta t}$ versus $1/P$ is a straight line, as shown by the data. For $1/P \to 0$, that is, $a \to \infty$, the noise along the path disappears [see Eq. (16)], hence the intercept with the vertical axis gives the residual width $\overline{\delta t}_0$ due only to the intial photon number (which is equal in all these cases).

In Fig. 9 we give data for an experimental situation where the initial voltage V_0 and final voltage V_1 applied to the EOM are fixed and the discharge is changed. Also in this situation, the average spread $\overline{\delta t}$ versus $1/P$ is a straight line.

Such a different experimental technique does not allow a direct evaluation of $\langle n_0 \rangle$, since the diffusion constant D is now changing from point to point with the discharge current. However, it permits us to reach points much closer to threshold and to show the linear dependence of $\overline{\delta t}$ versus $1/P$ even for P_s/P as large as 20.

The statistical time distributions have been collected over 300 s at a rate of 150 counts/s for a total of $M_0 = 4.5 \times 10^4$ counts. Each channel is affected by a relative counting error of the order of the reciprocal square root of the count number. This error will affect each moment by an amount evaluated in Ref. 24. Off course, increasing the measurement time would reduce the counting error, however, it would also introduce long-time drifts in some experimental parameters. Hence the
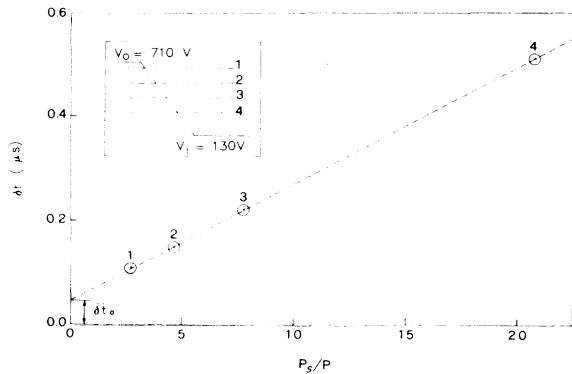

FIG. 9. Plot of $\overline{\delta t}$ vs $1/P$ for constant $\Delta k = k_0 - k_1 = 12.0 \times 10^6$ s^{-1} and variable gain Gz_0 (see inset). Error bars smaller than the dots as in Fig. 7. The gain at the four points are fixed by the following discharge currents: $i_1 = 3.377$ mA, $i_2 = 3.009$ ma, $i_3 = 2.800$ mA, and $i_4 = 2.599$ mA. The threshold current corresponding to $k_1 = k(V_1)$ is (2.480 ± 0.005) mA.

chosen counting time is a compromise between the two conflicting requirements. The counting error for the kth moment M_k is given by[24]

$$\epsilon_{M_k}^2 = \langle \delta M_k^2 \rangle = \frac{M_{2k} - M_k^2}{M_0} . \tag{31}$$

It is a straightforward matter to express the moments in terms of the cumulants. The error bar in $\overline{\delta t} \equiv \langle M_2 - M_1^2 \rangle^{1/2}$ is then given by

$$\delta(\overline{\delta t}) = \frac{\epsilon_{M_2} + 2\overline{t}(\overline{\delta t})/\sqrt{M_0}}{2\overline{\delta t}} , \tag{32}$$

where ϵ_{M_2} is easily evaluated in terms of all four cumulants K_1 to K_4,

$$M_4 - M_2^2 = K_4 + 4K_3 K_1 + 4K_2 K_1^2 - K_1^4 . \tag{33}$$

The error bar $\overline{\delta t} = \langle M_2 - M_1^2 \rangle^{1/2}$ is given by

$$\delta(\overline{\delta t}) = \frac{\epsilon_{M_2} + 2\overline{t}(\overline{\delta t})/\sqrt{M_0}}{2\overline{\delta t}} . \tag{34}$$

For instance, for the first of the three points in Fig. 7 we have

$$M_4 - M_2^2 = 1.64 \times 10^{-2} \ \mu s^4 ,$$

$$\epsilon_{M_2} = \frac{(1.64 \times 10^{-2})^{1/2}}{2 \times 10^2} = 0.65 \times 10^{-3} \ \mu s^2 .$$

Replacing in Eq. (34) we evaluate $\delta(\overline{\delta t}) = 1.55 \times 10^{-3}$ (μs) which corresponds to a relative error $\delta(\overline{\delta t})/\overline{\delta t} = 1.4 \times 10^{-2}$. Thus in all the reported measurements the relative error bars are of the order of 1–2 %, that is, smaller than the black denotation marks in Figs. 7 and 9.

Experiments on time jitter in semiconductor laser turn-on have been performed.[25] No direct comparison with our approach is possible for two reasons: (i) the transient in Ref. 25 develops over a picosecond range, hence the error bars are consistently larger than in our case; (ii) a fixed zero time reference is not easily accessible, hence there is no data for the average time. As a result, a model-independent approach like ours, based only on the knowledge of the first two cumulants, is not possible in that case. Furthermore, a preliminary observation of switching times in far ir laser was reported by Lefebvre et al.[26]

From Eq. (30) we can evaluate the relative error bar in N_0, that is,

$$\frac{\delta N_0}{N_0} = \overline{t}\delta a + a\delta(\overline{t}) + \frac{1}{\sqrt{n_1}} , \tag{35}$$

where $\delta a = 1.28 \times \delta(\overline{\delta t})/\overline{\delta t}^2$. By replacing the numerical values, the second and third term contribute only as 10^{-3} and 10^{-5}, respectively, whereas the first one yields a <u>30%</u> error bar (see Fig. 8). Since $\delta N_0/N_0$ varies as $1/\sqrt{M_0}$, to reduce this error to 3% we should increase the total number of counts by a factor 100. Once the relative error in N_0 has been calculated from the experimental data, use of Eq. (17) with the values of a and a_0 inferred from the

EOM voltages allows to establish the error in the diffusion coefficient and hence in the noise along the path n_p. It is easily proved that $\delta n_p/n_p = \delta D/D \simeq \delta N_0/N_0$. The corresponding data are collected in Table II and Fig. 7.

From Table II, the k_1 values associated with the three voltages V_1, summed up to the a values of the fourth line, yield by Eq. (3) a common value $Gz_0 = 34.3 \times 10^6$ s^{-1}. Since the value of G was calculated after Eq. (4), we can establish the following population inversion for the experiments of Fig. 3 and 4:

$$z_0 = 0.9 \times 10^{14} .$$

Furthermore, using the (practically uniform) D value of the last line and making use of Eqs. (8) and (9), we find for the total population of the upper level

$$N_2 = \frac{D}{\gamma_{sp}\eta} = 6.7 \times 10^{15} .$$

The error bar to be associated with this value is the sum of the error in D (about 30%) and the error in η (estimated to be around 20%). Hence this value of molecular population is highly accurate for the present standards.[20]

IV. DEVELOPMENT OF THE PHOTON PULSE AT INTERMEDIATE TIMES: THE TODA OSCILLATOR MODEL

As shown in the Sec. III, for photon numbers below the saturation value ($t \ll t_1$) the population inversion is constant and the dynamics is linear. Beyond t_1 the detailed interplay between photon number and population inversion must be taken into account.

A simple-minded approach in terms of a single mode field interacting with resonant two-level atoms with a large homogeneous broadening leads to the following equations:[18]

$$\dot{x} = -kx(1-z) , \tag{36}$$

$$\dot{z} = -\gamma(z + xz - \Delta_0) , \tag{37}$$

Here k and γ are, respectively, the loss rate of the cavity and the decay rate of the population inversion, and G is the coupling constant between photon and population number. The saturation photon number is given by

$$n_s = \frac{\gamma}{2G} \tag{38}$$

and the population inversion at threshold is given by k/G. Here x is the photon number n normalized to the saturation value, and z is the inversion number ΔN normalized to the threshold value, that is, $x = n/n_s$, $z = G\Delta N/k$. Similarly Δ_0 is the equilibrium value of z for $x = 0$.

We have to distinguish between two limit cases: $\gamma \gg k$ (so-called class-A lasers[11]) and $k \gg \gamma$ (class-B lasers). In the former case, we can neglect the time derivative in Eq. (36), which amounts to taking $z(t)$ adiabatically following the rather slow changes of $x(t)$. Thus $z = \Delta_0/(1+x)$. Replacing this into the photon equation the evolution is ruled by the single equation

$$\dot{x} = -kx + \frac{\Delta_0 x}{1+x} , \tag{39}$$

which yields no overshoots, as sketched in Fig. 10(a), and observed in Ref. 1 and 2. In the latter case and for an intermediate time range $k^{-1} \ll t \ll \gamma^{-1}$, we can assume that the Eq. (36) has reached equilibrium, which imposes $z \simeq 1$. If we now put $x = e^s$, $\dot{s} = \dot{x}/x$, Eq. (36) yields $\bar{s} = k\dot{z}$ and by use of the right-hand side of Eq. (37), already simplified with $z \simeq 1$, we obtain

$$\ddot{s} = \Delta_0 - 1 - e^s . \tag{40}$$

This is a lossless Toda oscillator, and its validity is limited to the time range where the giant spike develops. The heuristic argument here used to derive Eq. (40) is symbolized in Fig. 11(a), where it is shown that the chosen time interval corresponds to a decoupling from the atomic reservoir. A more general approach, developed by Oppo and Politi (Ref. 13) would also include damping terms, which, however, play no role in the considered time range.

The main qualitative difference is that it is impossible to approximate a class-B laser by a first order differential equation. The second-order character of Eq. (40) implies the development of a large peak (overshoot). This is the giant pulse usually associated with Q switching and which is absent in class-A lasers.

As discussed in Sec. II, up to t_1 there is no difference between class A and B, since the linear approximation yields $z = \Delta_0$ and

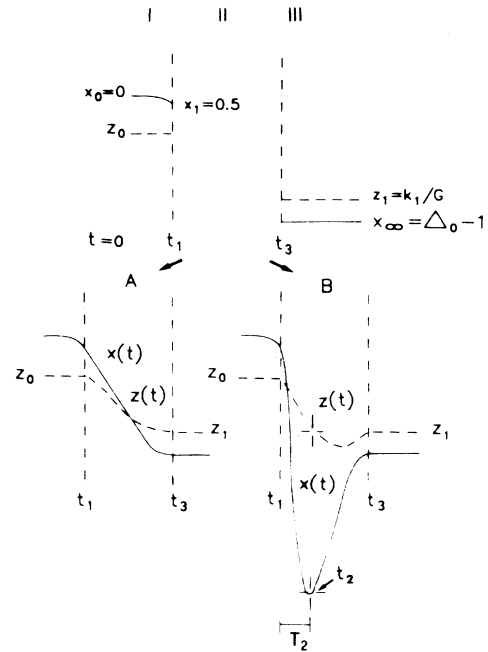$$\dot{x} = k(\Delta_0 - 1)x = ax , \tag{41}$$

FIG. 10. Schematic diagram of asymptotic (short-time and long-time) behavior, and main differences between class-A and class-B transients at intermediate times (region II).
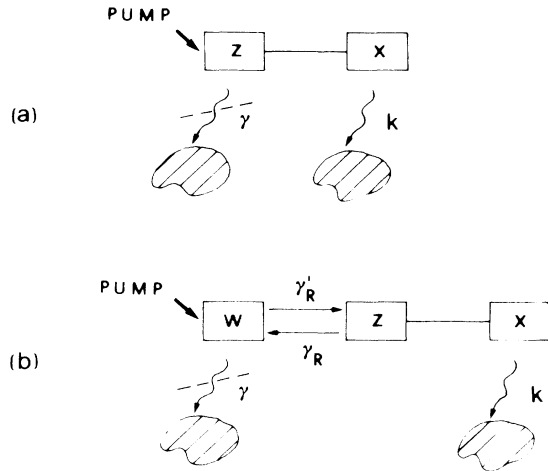
FIG. 11. (a) Conceptual scheme of the population (z) interaction with intensity (x) in a class-B_1 laser. The wavy lines denote the coupling with the thermal reservoirs (shadowed areas). Since $\gamma \ll k$ we can neglect the atomic (collisional) reservoir during the pulse formation (dashed line), so that the corresponding dynamics is purely radiative; (b) same for a class-B_2 laser. Here, z has a fast coupling with the vibrational manifold (w), which can be decoupled from its reservoir during the spike ($\gamma \ll k$). However, the coupling between z and w is effective during the pulse.

as the single evolution equation used in Sec. II. Beyond t_1, the nonlinear coupling between z and x plays a full role, and we can no longer use this linear approximation. While the class A Eq. (39) yields a monotonic increase of x and z, the class B Eq. (40) yields a large spike in the intensity. At the peak time t_2 the population has a value $z(t_2)=z_1$, followed by an undershoot below the asympotic value z_1 [Fig. 10(b)].

The Toda oscillator model Eq. (40) is in qualitative agreement with the experimental spikes reported on different time scales in Figs. 2, 5, and 6. In Ref. 13 there is a plot (Fig. 2) which displays in adimensional form the time T_1 that the Toda oscillator needs to go from a very small photon number to a photon number corresponding to $\ln x = -\ln(\Delta_0 - 1) = 1.6$ (since in our case $\Delta_0 = 1.2$), that is, to $x = 0.2$, which is near our threshold point $n_1 = 0.5 n_s$. We do not need to make use of T_1, since our treatment of Sec. III is more extensive, insofar as it accounts for the essential role of statistical fluctuations. More interesting is to make use of the T_2 value also plotted in Fig. 2 of Ref. 13. T_2 is the time that the pulse takes to develop from $x = 0.2$ to its peak. In order to perform a quantitative comparison we must introduce the same scaling as in Ref. 13. Thus we introduce a logarithmic translation $q = s - \ln(\Delta_0 - 1)$. In the new time scale

$$\tau = \sqrt{(\Delta_0 - 1)k\gamma}\, t \tag{42}$$

the equation of motion becomes simply

$$\ddot{q} = 1 - e^q . \tag{43}$$

Once we use the value $T_2 = 2$ coming from Fig. 2, Ref.

13, and our experimental values for $\Delta_0 k = k_1$, and γ, we obtain for the rise time T_2 [time interval between t_1 and the peak position t_2 as shown in the scheme of Fig. (10)]

$$T_2 \simeq 12 \ \mu s ,$$

which is wrong by a factor of 10 with respect to the experimental value $T_2 \sim 1 \ \mu s$. To provide a quantitative agreement, we modify our B_1 (or two-level) model into a B_2 (four-level) model, which accounts for the coupling of the active transition having population inversion z with a large rotational manifold, described by an overall population difference w. The detailed equations will be given in Sec. V. Here it is sufficient to say [see Fig. 11(b)] that since the relaxation rates γ_R and γ'_R from z to ω and from w to z are of the same order as k, during the time range over which $z \simeq 1$, also w is clamped rigidly to the ratio γ_R / γ'_R, that is, $w \simeq 16$.

Such a drastic assumption corresponds to a temporary freezing of the molecular population during the rise time of the radiation pulse. Precisely for $t_1 < t < t_2$ the total manifold $w + z$ has equilibrated within itself (this equilibration requires a time $\gamma_R^{-1} < t_1$) and it is still decoupled from the thermal bath (the thermal relaxation would take the much longer time γ^{-1}).

Redoing the same steps as for Fig. 11(a) we easily arrive at the equation

$$\frac{\ddot{s}}{k\mu} = \Delta_0 - e^s \simeq 1 - e^s \tag{44}$$

Here, $\mu \simeq Z\gamma$, where $Z = 16$ is the effective number of rotational levels. Notice that Eq. (44) looks like Eq. (43), thus we must use the same value $T_2 = 2$ of Ref. 13, how-
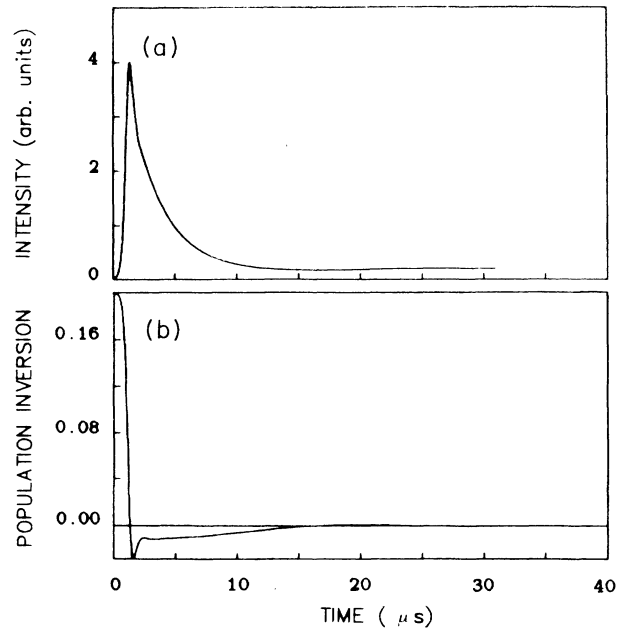

FIG. 12. Numerical solutions for class-B_2 laser transient. (a) Photon number, (b) population inversion.

ever, with a new time scale $\tau' = \sqrt{k\mu} t$. We obtain

$$T_2' = \frac{2}{\sqrt{k\mu}} \simeq 1.1 \ \mu s \ ,$$

in good agreement with the experimental result. This proves the essential role of the coupling within the rotational manifold.

V. LONG TIME BEHAVIOR: CLASS-B_2 VERSUS CLASS-B_1 LASERS

The experimental plot of the long-time evolution (Fig. 6) has shown the clear character of the class B laser. However, Eq. (40) or its B_2 equivalent is useless beyond the peak of the photon pulse (that is, beyond 4 μs) and
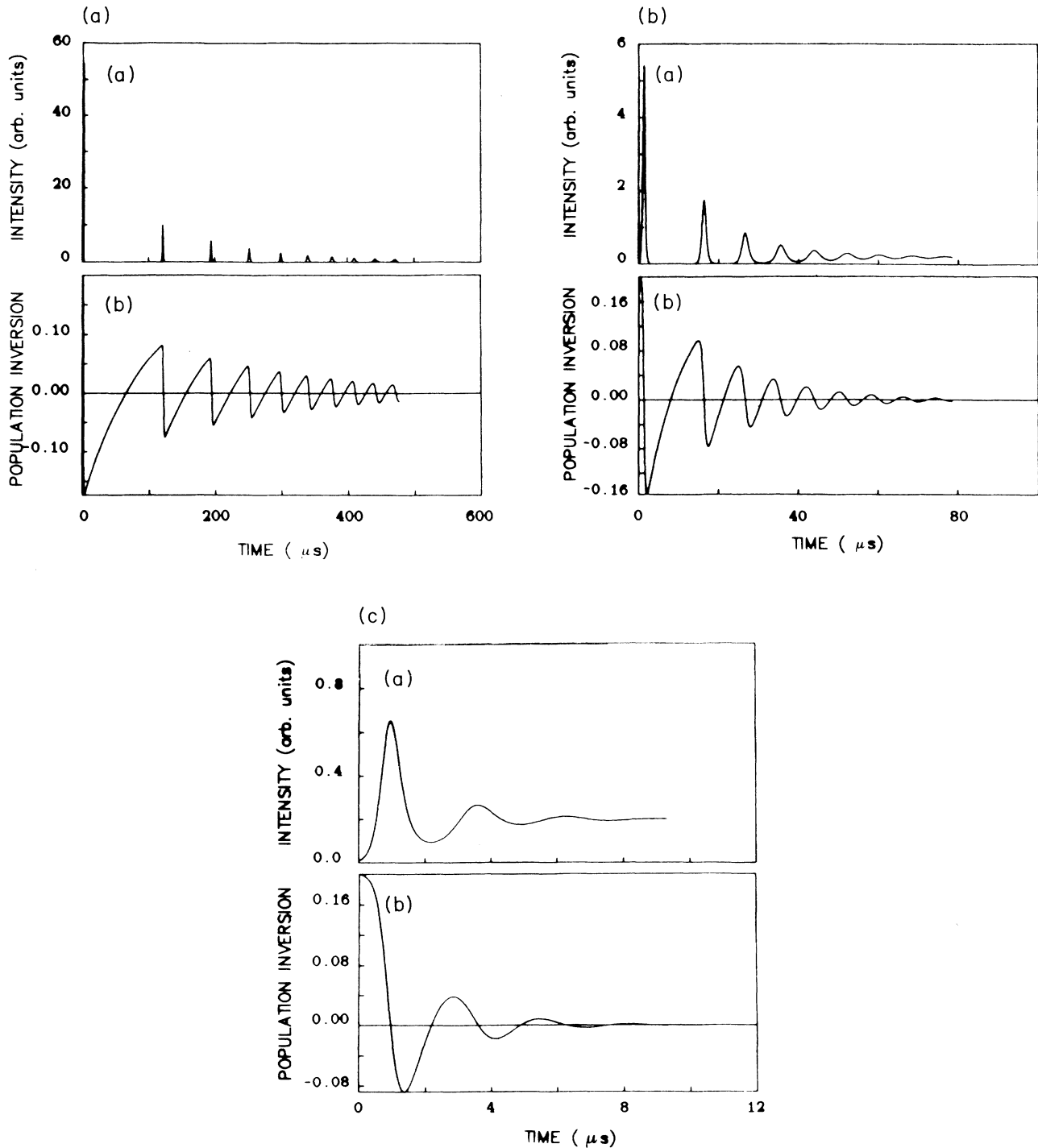

FIG. 13. Numerical solutions for photon number and population inversion in a class-B_1 laser transient for three different γ values, that is, (a) 10^4, (b) 10^5, and (c) 10^6 s^{-1}.

full use of the laser equations must be made in order to trace the role of the population decay to its thermal reservoir.

While Eqs. (36) and (37) are accurate for ruby or Nd lasers (class B_1) they are inadequate for the CO_2 laser (class B_2). The radiative transition is just one among the many of the rotational manifold. This transition, besides the long-time collisional decay out of the vibrational band, has a much faster coupling with the other levels of the same band. To describe this compound molecular decay we must resort to a four-level scheme[14,15] which implies the following rate equations:

$$\dot{x} = -kx(1-z) , \tag{45}$$

$$\dot{z} = -(\gamma_R + \gamma)z + \gamma_R' w - \mu xz + \eta\gamma\Delta_0 , \tag{46}$$

$$\dot{w} = -(\gamma_R' + \gamma)w + \gamma_R z + (Z-1)\eta\gamma\Delta_0 . \tag{47}$$

Here, x and z are the photon and radiative populations, normalized as before, w is the overall population inversion between upper and lower vibrational bands diminished by z ($w + z$ is the total population inversion, of which only z is radiatively active), γ_R is the decay rate from z to w, γ_R' is the decay rate from w to z,

$$\mu = \gamma(\gamma_R + \gamma_R' + \gamma)/(\gamma_R' + \gamma) , \tag{48}$$

and

$$\eta = (\gamma_R + \gamma_R' + \gamma)/(\gamma R + \gamma) , \tag{49}$$

Here we have used a modified set of equations with respect to those of Ref. 15, in order to have the correct asymptotic values for long times.[27]

Notice that the two intraband coupling rates are related as

$$\gamma_R = Z\gamma_R' , \tag{50}$$

where Z is of the number of effective rotational levels. It depends on the discharge pressure and current. In our case[27] we fit our data with $Z = 16$.

Equations (45)–(47) show that the saturation photon number is given by

$$n_s = \frac{\mu}{2G} \tag{51}$$

instead of Eq. (38). The numerical difference is relevant ($\mu/\gamma \simeq Z$), and it was the basis of the correction to the spike position in time (Sec. IV).

Figure 12 shows the evolution of x and z for the class B_2 laser. A best fit with our experimental data of Fig. 6 gives the following decay rates (in s^{-1}):

$$\gamma_R = 0.5 \times 10^7, \quad \gamma_R' = 0.6 \times 10^6, \quad \gamma = 10^4 .$$

If we try to approximate the time development by class-B_1 equations with $\gamma = 10^4$, we obtain numerical data rather different from the experimental ones. Increasing γ to 10^6 we reach a fair agreement on the giant pulse, but we have also a damped oscillation (Fig. 13) absent in the experiment. The multipeaked structure of Q switching obtained numerically for $\gamma = 10^4$ or 10^5 was indeed observed in Q-switched class B_1 lasers.[28] Notice that, for long times, the depletion of the rotational manifold may induce relevant perturbation in long-time instabilities, thus requiring a still different model.[29] However, in the time range interesting for our experimental investigation the model we have used seems to be in satisfactory agreement with our laboratory data.

The question whether a global model might cover all possible ranges and describe all the relevant physics of the CO_2 laser remains still open. We observe, however, that more sophisticated modeling should account also for plasma phenomena in the discharge, thus reaching a complexity which would strongly limit its usefulness. Hence it is still more useful to apply "local" models which explain a well defined range of phenomena, as we did here.

ACKNOWLEDGMENTS

*Also at Department of Physics, University of Florence, Italy.

†Permanent address: University of Warsaw, Warsaw, Poland.

‡Permanent address: Universidade Estadual de Campinas, Campinas, São Paulo, Brazil.

[1]F. T. Arecchi, V. Degiorgio, and B. Querzola, Phys. Rev. Lett. 19, 1168 (1967).

[2]F. T. Arecchi, and V. Degiorgio, Phys. Rev. A 3, 1108 (1971).

[3]R. Kubo, in Synergetics, edited by H. Haken (Teubner, Stuttgart, 1973), pp. 28–44.

[4]F. Haake, Phys. Rev. Lett. 41, 1685 (1978).

[5]M. Suzuki, in Order and Fluctuations in Equilibrium and Nonequilibrium Statistical Mechanics, XVII International Solvay Conference on Physics, edited by G. Nicolis, G. Dewel, and J. W. Turner (Wiley, New York, 1981), pp. 299–365.

[6]F. T. Arecchi, in Order and Fluctuations In Equilibrium and Nonequilibrium Statistical Mechanics, XVII International Solvay Conference on Physics, edited by G. Nicolis, G. Dewel, and J. W. Turner (Wiley, New York, 1981), pp. 107–157.

[7]F. T. Arecchi and A. Politi, Phys. Rev. Lett. 45, 1219 (1980).

[8]F. T. Arecchi, A. Politi, and L. Ulivi, Nuovo Cimento 71B, 119 (1982).

[9]R. Roy, A. W. Yu, and S. Zhu, Phys. Rev. Lett. 55, 2794 (1985).

[10]S. Zhu, A. W. Yu, and R. Roy, Phys. Rev. A 34, 4333 (1986).

[11]F. T. Arecchi, G. L. Lippi, G. P. Puccioni, and J. R. Tredicce, Opt. Commun. 51, 3081 (1985).

[12]F. Haake, J. W. Haus, and R. Glauber, Phys. Rev. A 23, 3255 (1981); F. de Pasquale, J. M. Sancho, M. San Miguel, and P. Tartaglia, Phys. Rev. Lett. 56, 2473 (1986).

[13]G. L. Oppo and A. Politi, Z. Phys. B **59**, 111 (1985).

[14]J. Dupré, F. Meyer, and C. Meyer, Rev. Phys. Appl. (Paris) **10**, 285 (1975).

[15]E. Arimondo, F. Casagrande, L. A. Lugiato, and P. Glorieux, Appl. Phys. B **30**, 57 (1983).

[16]E. Arimondo, D. Dangoisse, G. Gabbanini, E. Menchi, and F. Papoff, J. Opt. Soc. Am. B **4**, 892 (1987).

[17]F. T. Arecchi, R. Meucci, and J. A. Roversi, Europhys. Lett. **8**, 225 (1989).

[18]F. T. Arecchi, in *Instabilities and Chaos in Quantum Optics,* edited by F. T. Arecchi and R. G. Harrison (Springer-Verlag, New York, 1987), p. 9.

[19]W. H. Louisell, *Quantum Statistical Properties of Radiation* (Wiley, New York, 1973).

[20]P. K. Cheo, *Lasers,* edited by A. K. Levine and A. J. DeMaria (Dekker, New York, 1976), Vol. 3, p. 134.

[21]E. B. Rockower, N. B. Abraham, and S. R. Smith, Phys. Rev. A **17**, 1100 (1978).

[22]*Handbook of Mathematical Functions,* edited by M. Abramowitz and I. A. Stegun (Dover, New York, 1965), p. 258.

[23]M. C. Torrent and M. San Miguel, Phys. Rev. A **38**, 245 (1988).

[24]F. T. Arecchi, in *Quantum Optics,* Proceedings of the International School of Physics "Enrico Fermi," edited by R. J. Glauber (Academic, New York, 1969), p. 57.

[25]P. Spano, A. D'Ottavi, A. Mecozzi, and B. Daino, Appl. Phys. Lett. **52**, 2203 (1988); A. Mecozzi, S. Piazzolla, A. D'Ottavi, and P. Spano, Phys. Rev. A **38**, 3136 (1988).

[26]M. Lefevbre, P. Bootz, D. Dangoisse, and P. Glorieux, in *Laser Spectroscopy,* edited by H. P. Weber and W. Luthy (Springer, Berlin, 1983) p. 282.

[27]F. T. Arecchi, W. Gadomski, R. Meucci, and J. A. Roversi, Opt. Commun. **65**, 47 (1988).

[28]F. T. Arecchi, G. Potenza, and A. Sona, Nuovo Cimento **34**, 1458 (1964).

[29]M. Tachikawa, K. Tanii, and T. Shimizu, J. Opt. Soc. Am. B **5**, 1077 (1988).